Pacemaker activity resulting from the coupling with nonexcitable cells

Vincent Jacquemet*

Signal Processing Institute, Ecole Polytechnique Fédérale de Lausanne (EPFL), CH–1015 Lausanne, Switzerland

Fibroblasts are nonexcitable cells that are sometimes coupled with excitable cells (cardiomyocytes). Due to a higher resting potential, these cells may act as a current source or sink and therefore disturb the electrical activity of the surrounding excitable cells. The possible occurrence of spontaneous pacemaker activity resulting from these electrotonic interactions was investigated in a theoretical model of two coupled cells as well as in a multicellular fiber model based on the Courtemanche kinetics. The results indicate that repeated spontaneous activations can be observed after an alteration in the activation and recovery properties of the sodium current (changes in excitability properties), provided that the difference in the resting potential as well as the coupling between the excitable and nonexcitable cells is sufficiently high. This may constitute a mechanism of focal sources triggering arrhythmias such as atrial fibrillation.

PACS number(s): 87.10.+e, 87.19.Hh, 87.16.Ac, 87.19.Nn

I. INTRODUCTION

Atrial fibrillation (AF) is the most frequent rhythm disorder observed in the human heart. Typically, AF is characterized by multiple spinning electrical wavelets traveling over both atria, causing these upper chambers to quiver at a rate of 300 to 600 times per minute. Invasive, electrophysiological studies have identified one subform of AF having its origin located in the pulmonary veins [1]. The conceptual description underlying this type of AF postulates that AF is triggered and perpetuated by one or several sources of ectopic beats (focal activity). The mechanism of spontaneous firing in the pulmonary vein region so far has remained unclear.

The increase of AF prevalence with age [2] has prompted the investigation of the effects of structural and functional changes associated with aging, such as fibrosis [3–5]. Cardiac fibrosis is marked by the formation of fibrous tissue in the lining and the muscle of the heart [6]. This fibrous tissue is composed of nonexcitable cells, the fibroblasts, characterized by a higher resting potential than that of the myocytes [7]. Since fibroblasts can be coupled through gap junctions with other fibroblasts as well as to myocytes [8], they may act as a current sink or source for the electrical activity in the latter and therefore disturb the propagation of the cardiac impulse.

Dissections of human autopsy hearts demonstrated myocardial sleeves extending the left atrial myocardium along the pulmonary veins [9]. The distal zones of these sleeves showed increased fibrous tissue, presumably providing a substrate for microreentries and ectopic foci [9]. Inspired by the work of Fenton *et al.*, analyzing the occurrence of spontaneous activations produced by differences in resting potentials [10], we hypothesized that, under specific pathological conditions, pacemaker activity can occur if a group of atrial cells is coupled with nonexcitable cells (fibrous tissue) characterized by a higher resting potential. A similar mechanism was proposed by Keener to describe the onset of ventricular fibrillation following coronary artery occlusion [11]. This might constitute a mechanism of focal sources triggering AF.

In this paper, the basic mechanisms describing the occurrence of a spontaneous pacemaker activity are first investigated in a simplified model of two coupled cells enabling an analytical study of its dynamics and the identification of the most important parameters affecting its qualitative behavior. Then, numerical simulations are performed to extend the results to a one-dimensional tissue model with more realistic membrane properties.

II. BASIC MECHANISMS

We first consider two coupled cells (one excitable cell and one nonexcitable cell) with transmembrane potentials u_1 and u_2. Assuming a linear coupling due to the presence of gap junctions, their evolution is governed by the equations [12]

$$C_1 \frac{du_1}{dt} = -I_1(u_1, \mathbf{w}_1) - \tilde{g}(u_1 - u_2), \tag{1}$$

$$C_2 \frac{du_2}{dt} = -I_2(u_2, \mathbf{w}_2) - \tilde{g}(u_2 - u_1), \tag{2}$$

where, for $i = 1, 2$, C_i is the membrane capacitance (in μF), I_i is the (outward) ionic current through the cell membrane (in μA), $\mathbf{w}_i$ describes the membrane state (i.e., internal variables such as the probability for an ion channel to be open), and $\tilde{g}$ is the coupling conductance (in μS). The membrane current of the first cell is specified by the FitzHugh-Nagumo model [13–16]

$$I_1(u_1, w_1)/C_1 = -ku_1(u_1 - a)(1 - u_1) + w_1, \tag{3}$$

where k and a are positive parameters. This model includes a single internal variable w_1 whose dynamics is governed by the equation

$$\frac{dw_1}{dt} = \epsilon(u_1 - \gamma w_1), \tag{4}$$

where ϵ and γ are two positive parameters. Since the second cell is taken to be nonexcitable, I_2 can be modeled as

---

*Email address: vincent.jacquemet@a3.epfl.ch

$$I_2(u_2) = g_m(u_2 - u_0), \tag{5}$$

where u_0 is its equilibrium potential and g_m is the membrane conductance.

In the sequel of this section, we assume that g_m is large ($g_m \to \infty$). By reducing by one the number of dynamical variables as well as the number of parameters, this assumption enables us to determine analytically the exact dynamical behavior of a simplified system that qualitatively captures some of the features of the complete coupled system. In this situation, $u_2 \approx u_0$ and the system (1)–(5) is approximated by two coupled differential equations in u_1 and w_1. With the indices 1 skipped for the sake of clarity, this system reads

$$\frac{du}{dt} = p(u) - w, \tag{6}$$

$$\frac{dw}{dt} = \epsilon(u - \gamma w). \tag{7}$$

The function $p(u)$ is a third-order polynomial (with negative leading coefficient) defined as

$$p(u) = ku(u - a)(1 - u) - g(u - u_0), \tag{8}$$

where $g = \tilde{g}/C_1$. Note that introducing a coupling g between the cells only results in a change of the coefficients of the polynomial.

The resting potential u^* of the coupled system is one of the stable fixed points of Eqs. (6) and (7). A fixed point (u^*, w^*) is a solution of

$$p(u^*) - u^*/\gamma = 0 \quad \text{and} \quad w^* = u^*/\gamma. \tag{9}$$

Solving Eq. (9) requires extracting the real root(s) of a third-degree polynomial. At least one real root exists. In order to avoid nonphysiological conditions, the parameters k, a, γ, g, and u_0 were chosen such that indeed a unique simple real root exists. If this fixed point becomes unstable, a limit cycle is generally observed for asymptotically long times, since only these two types of attractor can exist in two dimensions (according to the Poincaré-Bendixon theorem) [16].

The stability of the fixed point is governed by the eigenvalues of the Jacobian matrix

$$J(u^*) = \begin{pmatrix} \alpha & -1 \\ \epsilon & -\epsilon\gamma \end{pmatrix}, \tag{10}$$

where α is defined as the derivative of the polynomial at u^*, i.e., $\alpha = p'(u^*)$. The fixed point is linearly stable if the real part $\operatorname{Re}\lambda_\pm$ of the eigenvalues $\lambda_\pm$ of $J(u^*)$ is negative. These eigenvalues are given by

$$2\lambda_\pm = \alpha - \epsilon\gamma \pm \sqrt{\Delta}, \tag{11}$$

$$\Delta = (\epsilon\gamma - \alpha)^2 - 4\epsilon(1 - \alpha\gamma). \tag{12}$$

If $\alpha - \epsilon\gamma \geq 0$, then $\operatorname{Re}\lambda_+ \geq 0$ and the fixed point is unstable. So we assume that $\alpha - \epsilon\gamma < 0$. If $\Delta < 0$, the eigenvalues are complex with a negative real part, so that the fixed point is stable and the transient dynamics is characterized by damped oscillations. This happens when
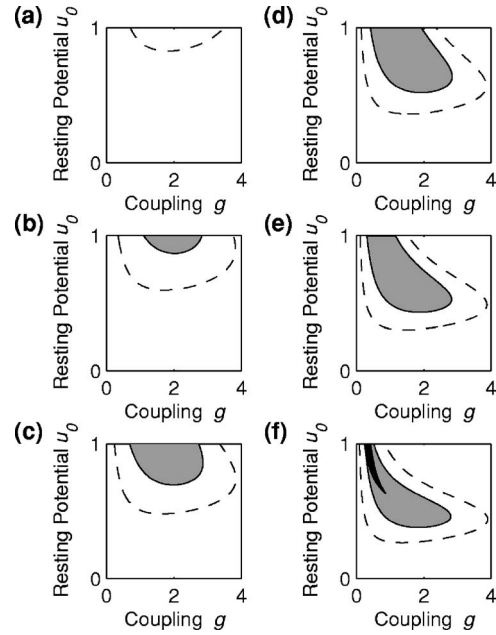

FIG. 1. Bifurcation diagrams for different values of the recovery parameter γ: (a) $\gamma = 0.1$, (b) $\gamma = 0.15$, (c) $\gamma = 0.2$, (d) $\gamma = 0.3$, (e) $\gamma = 0.4$, and (f) $\gamma = 0.5$. The gray region corresponds to pacemaker activity, the white region to a stable resting potential, and the black region to nonphysiological conditions. The dashed line determines the region with transient oscillations.

$$-\epsilon\gamma - 2\sqrt{\epsilon} < \alpha < -\epsilon\gamma + 2\sqrt{\epsilon}. \tag{13}$$

If $\Delta \geq 0$, we have to check whether λ_+ (which is real) can be positive. This occurs when $\alpha > \gamma^{-1}$. When $\alpha \leq \gamma^{-1}$, the fixed point is stable.

Thus, the stability of the fixed point $(u^*, u^*/\gamma)$ only depends on the parameter $\alpha(u^*)$. A phase transition can occur at $\alpha = \epsilon\gamma$, $\alpha = \gamma^{-1}$, and $\alpha = -\epsilon\gamma \pm 2\sqrt{\epsilon}$. We need to arrange these values in ascending order to determine the qualitative behavior of the system as a function of α. For this purpose, we will assume that $\epsilon < \gamma^{-2}$. The rationale for this assumption is that a small ϵ leads to a stiffer system, characterized by a steep depolarization followed by a slower repolarization. This is what we would expect for cardiac cells. Under this assumption, we have

$$-\epsilon\gamma - 2\sqrt{\epsilon} < \epsilon\gamma < -\epsilon\gamma + 2\sqrt{\epsilon} < 1/\gamma, \tag{14}$$

and the fixed point $(u^*, u^*/\gamma)$ is unstable when $\alpha(u^*) \geq \epsilon\gamma$, stable when $\alpha(u^*) < \epsilon\gamma$, and stable with damped oscillations (complex eigenvalues) when $-\epsilon\gamma - 2\sqrt{\epsilon} < \alpha(u^*) < \epsilon\gamma$.

Figure 1 displays examples of bifurcation diagrams, with the model parameters set to $k = 10$, $a = 0.15$, $\epsilon = 0.2$, $0.1 \leq \gamma \leq 0.5$. These parameters were selected so that $\epsilon < \gamma^{-2}$ and no spontaneous activation occurs in the absence of coupling. For each pair of parameters (g, u_0) in the range $0 \leq g \leq 4$ and $0 \leq u_0 \leq 1$, the asymptotic behavior of the system is either periodic (limit cycle) or constant (stable fixed point). The gray region corresponds to a limit cycle and the white region to a stable fixed point. The dashed line determines the region with transient oscillations (complex eigenvalues with nega-
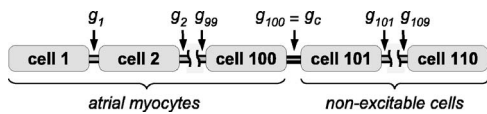
FIG. 2. Schematic representation of the multicellular fiber model.

tive real part). The black region in the right bottom panel of Fig. 1 corresponds to three fixed points, a clearly nonphysiological situation. From this figure, it appears that (1) if the coupling is very weak (if g is small), the dynamics is similar to that of an isolated excitable cell; (2) if the coupling is very strong (if g is large), the cell remains at a constant potential close to that of the nonexcitable cell; (3) for intermediate coupling coefficients, a periodic activity will appear spontaneously; (4) a critical, sufficiently high resting potential u_0 is required for this periodic activity; (5) this critical resting potential depends on the recovery properties of the cell (the parameter γ).

III. A MULTICELLULAR FIBER MODEL

The simplified model of two coupled cells described in the previous section provided a qualitative understanding of the possible changes in the dynamics (bifurcations) of an excitable system arising as a consequence of its coupling with a nonexcitable system. In order to study the electrophysiological conditions for which similar phenomena could be observed in the pulmonary veins in the presence of fibrosis, a unidimensional multicellular fiber model is considered. The high number of parameters involved in this more detailed model prevents a comprehensive systematical scanning of their values and their impact. The ones selected for further analysis (resting potential and coupling) in this section were inspired by the results of the preceding simpler model.

The multicellular fiber model consists of 110 cells connected through gap junctions. The first 100 cells represent cardiac myocytes and the last 10 cells represent nonexcitable cells. The transmembrane potential u_i of the ith cell satisfies the following cable equation generalizing (1):

$$C_i \frac{du_i}{dt} = - I_i(u_i) - g_{i-1}(u_i - u_{i-1}) - g_i(u_i - u_{i+1}), \quad (15)$$

where C_i is the membrane capacitance of cell i, I_i is the ionic current through the cell membrane, and g_i is the coupling conductance between cell i and $i+1$ (see Fig. 2). A no-flux boundary condition was assumed at the extremities of the fiber. This setup is similar to heterogeneous cell culture models with strands of cardiomyocytes [17]. In order to limit the number of adjustable parameters, the coupling constants g_i/C_i were given a uniform value 25 nS/pF, for which the cardiac impulse propagates at a velocity of about 80 cm/s (if the cells are 100 μm long). The coupling constant g_{100}, denoted hereafter by g_c, describes the coupling between the myocytes and the nonexcitable cells; it was set to different values within the range from 0 to 15 nS/pF.

The dynamics of the cardiac cells is described by the Courtemanche et al. [18] atrial cell model which takes into

account 12 membrane currents (Na$^+$ currents: I_{Na}, $I_{Na,b}$; K$^+$ currents: I_{K1}, I_{to}, I_{Ks}, I_{Kr}, I_{Kur}; Ca^{2+} currents: $I_{Ca,L}$, $I_{p,Ca}$, $I_{Ca,b}$; pumps and ion exchangers: I_{NaK}, I_{NaCa}), variations in ionic concentration (Na$^+$, K$^+$, and Ca^{2+}) and the intracellular Ca^{2+} dynamics related to its store in the sarcoplasmic reticulum. This resulted in a system of 21 differential equations. The aggregate current I_i/C_i is the sum of the 12 membrane currents mentioned above (in Ref. [18], those currents are given in pA/pF). In order to adapt the Courtemanche et al. model to the electrophysiological properties of the pulmonary vein myocytes, the currents I_{to} and I_{K1} were reduced by 25% and 40%, respectively, and the delayed rectifier currents I_{Ks}, I_{Kr}, and I_{Kur} were increased by 60%, 50%, and 50%, in agreement with patch-clamp measurements of canine pulmonary vein cardiomyocytes [19]. The L-type Ca^{2+} current was reduced by 70% so that the effective refractory period was about 180 ms, a value within physiological range (177±43 ms measured using a catheter in the pulmonary veins of patients with paroxysmal AF [20]).

The effects of the alteration of the myocyte excitability properties were studied by modifying the fast inward Na$^+$ current. This current was formulated as $I_{Na}(u) = g_{Na}m^3hj(u - E_{Na})$, where g_{Na} is the ion channel conductance, E_{Na} is the reversal potential, and m, h, and j are three gating variables [18]. Each gating variable satisfies an equation of the form

$$\frac{dy}{dt} = - \frac{y - y_\infty(u)}{\tau_y(u)} \quad (16)$$

describing the process of opening and closing of ion channel gates, in which y stands for m, h, and j. The voltage dependence of the functions $y_\infty(u)$ and $\tau_y(u)$ was shifted. More precisely, the original functions $m_\infty(u)$ and $\tau_m(u)$ were replaced by $m_\infty(u - \Delta V_{exc})$ and $\tau_m(u - \Delta V_{exc})$ respectively. A negative shift ($\Delta V_{exc} < 0$) resulted in a decrease of the excitation threshold. Similarly, $h_\infty(u)$, $\tau_h(u)$, $j_\infty(u)$, and $\tau_j(u)$ were shifted by ΔV_{rec}. This operation altered the recovery of the Na$^+$ current. Values for the parameters ΔV_{exc} and ΔV_{rec} were selected in the range −8.5 to 0 mV and −1 to 3 mV respectively.

The membrane current in nonexcitable cells was modeled by $I_i(u_i) = g_m(u_i - u_0)$ as in Eq. (5). Passive electrophysiological properties of cardiac fibroblasts have been documented in the literature, mainly for the rat heart. The membrane resistance values of fibroblasts were found to lie in the gigaohm range (0.51–3.8 GΩ in rat atrium [7], and 5.5±0.6 GΩ in rat ventricles [21]). Shibukawa et al., reported a membrane capacitance of 4.5±0.4 pF for ventricular fibroblasts [21]. In the model, $g_m/C_i = 0.1$ nS/pF was chosen as a baseline value. The resting potential can vary significantly from cell to cell: values in the range of −70 to 0 mV have been reported [21,7]. In the model, the resting potential u_0 of all the nonexcitable cells was set to the same value, selected from the interval −55 to −30 mV.

The system of ordinary differential equations (15) was solved numerically using a Crank–Nicholson scheme with a time step of 10 μs.
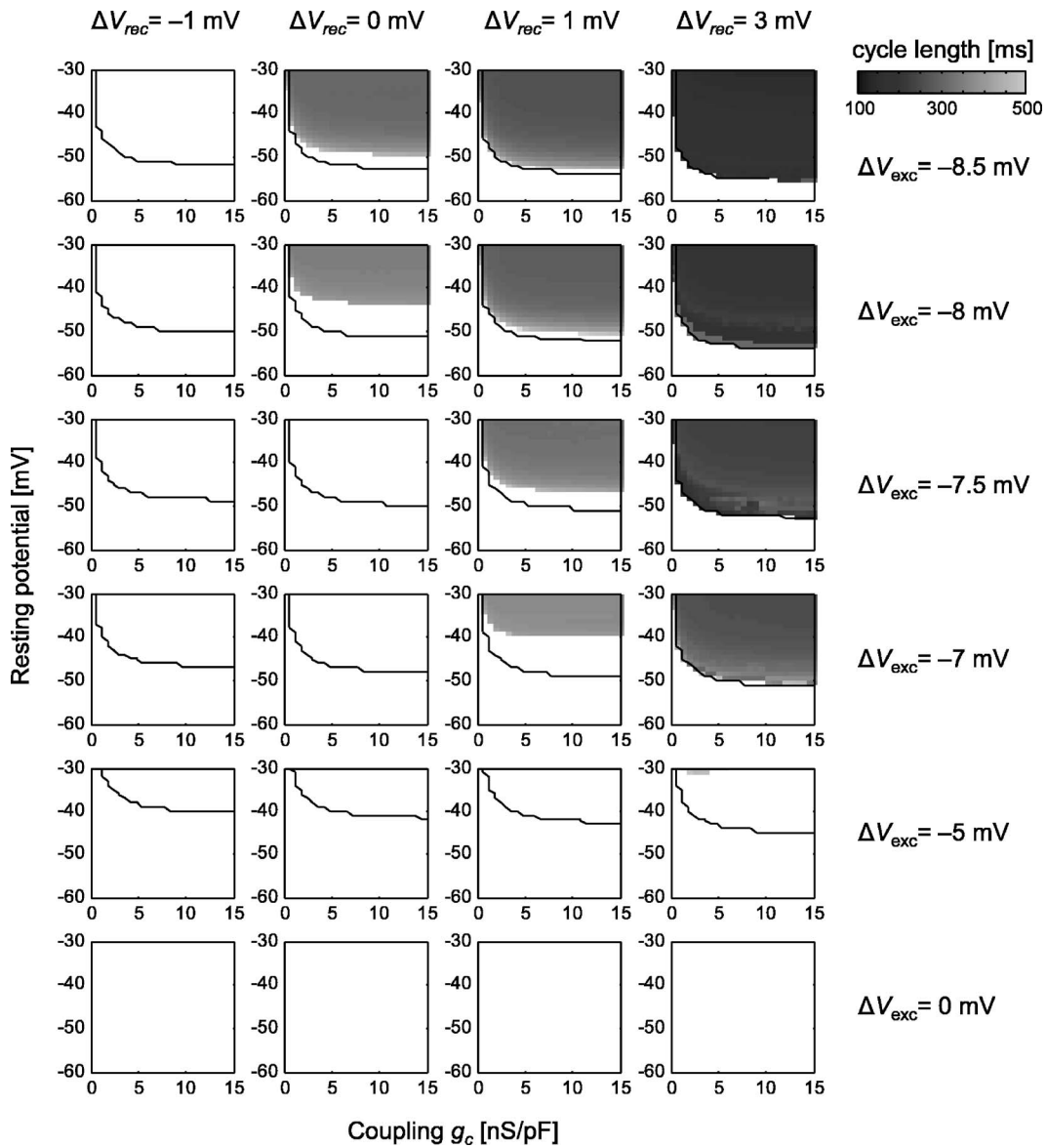
FIG. 3. Bifurcation diagrams of the spontaneous activity of the multicellular fiber model. Each column corresponds to a value of ΔV_{rec} and each row to a value of ΔV_{exc}. In the bifurcation diagrams, the region above the continuous line is characterized by at least one spontaneous activation. When pacemaker activity was detected, the mean cycle length is displayed using gray level coding.

IV. BIFURCATION DIAGRAMS

For each selection of the parameters ΔV_{exc} and ΔV_{rec}, a bifurcation diagram was computed according to the following protocol. The coupling coefficient (g_c) and the resting potential of the nonexcitable cells (u_0) were considered as control parameters and were successively given a value from 0 to 15 nS/pF (step: 0.6 nS/pF) and from −60 to −30 mV (step: 1 mV) in order to scan the parameter space. For each pair of parameters (g_c, u_0), the evolution of the multicellular fiber model was simulated for 5 s, starting with all cells at their resting state. The activations of cell 1 (located at the extremity of the fiber, see Fig. 2), if any, were detected. The dynamical behavior was classified into three categories: (1) no spontaneous activation, (2) one single spontaneous activation, and (3) repeated spontaneous activations (pacemaker

activity). When repeated activations were observed for at least 5 s, the mean cycle length was computed.

Figure 3 displays the resulting bifurcation diagrams. No activation was observed in the absence of coupling ($g_c=0$). This confirms the stability of the resting potential for the isolated atrial cell model, even with an altered Na$^+$ current. In the presence of coupling ($g_c>0$), but without alteration of the excitability properties of the atrial cells (last row of Fig. 3), a stable profile of resting potential was created by electrotonic effects after the steady-state was reached. Figure 4 shows this profile for different values of the coupling parameter g_c and the resting potential u_0 of the nonexcitable cells. Note that the resting potential of the nonexcitable cells can be significantly lower than the resting potential u_0 of the same cells when isolated.
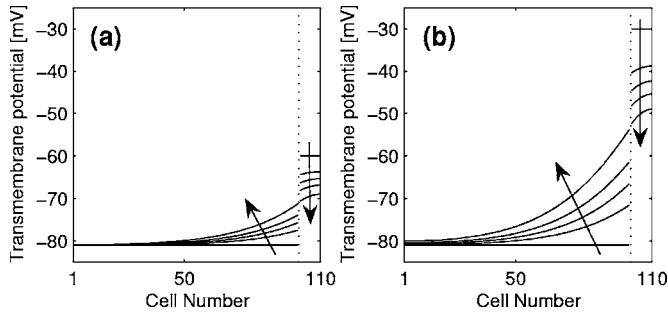
FIG. 4. Steady-state profiles of transmembrane potential along the fiber. The resting potential of the nonexcitable cells (when isolated) is (a) $u_0 = -60$ mV and (b) $u_0 = -30$ mV. The vertical dotted line represents the transition between atrial cells (on the left) and nonexcitable cells (on the right). Profiles are shown for different values of the coupling conductance: $g_c = 0$, 0.3, 0.6, 1.25, 15 nS/pF, respectively, in the order indicated by the arrows.

When the excitation threshold was decreased ($\Delta V_{exc} < -3$ mV), a single activation having its origin at the junction between the excitable and nonexcitable cells occurred for sufficiently high values of the resting potential u_0 (row 5 of Fig. 3). This happened because the steady-state resting potential became higher than the excitation threshold. However, after the depolarization, the transmembrane potential did not return to a sufficiently low level to reopen the Na$^+$ inactivation gates, so that activations were no longer possible [10]. A further decrease of the excitation threshold ($\Delta V_{exc} < -7.5$ mV, see row 2 of Fig. 3) enabled pacemaker activity to appear, with cycle lengths around 300–400 ms, because the lack of open inactivation gates was compensated by a higher excitability. When the recovery threshold for the Na$^+$ inactivation gates was increased ($\Delta V_{rec} > 0$), pacemaker activity was observed at a lower resting potential u_0 (columns 3 and 4 vs column 2 of Fig. 3). The resulting cycle length was found to be shorter (140 to 300 ms). In contrast, no repeated activation was observed when the recovery threshold was reduced ($\Delta V_{rec} < 0$).

The existence and the spread of the region of pacemaker activity in the bifurcation diagrams can be explained as follows in terms of steady-state inward sodium current (the so-called "window current") [11]. This current is given by

$$\bar{I}_{Na} = g_{Na} m_\infty^3 (u - \Delta V_{exc}) h_\infty (u - \Delta V_{rec}) j_\infty (u - \Delta V_{rec})(u - E_{Na}),$$
(17)

and determines the cell excitability as a function of the resting potential [11]. The window current is important because the resting potential spans a range of transmembrane potential in the transition zone (see Fig. 4). In order to enable a reexcitation of the cell, there must exist an interval of resting potential for which the window current is nonnegligible. Figure 5 displays the peak window current (in absolute value) as a function of the parameters ΔV_{exc} and ΔV_{rec}. Comparison with Fig. 3 shows that higher values of the peak window current are associated with the occurrence of pacemaker activity.
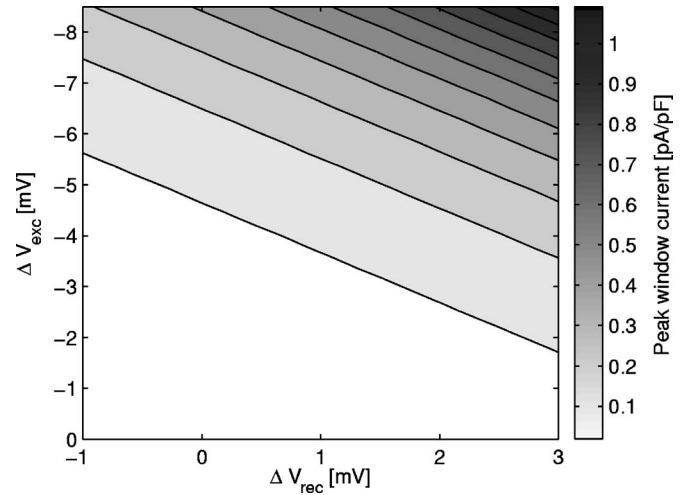

FIG. 5. Peak window current $\bar{I}_{Na}$ gray level coded as a function of the excitability parameters ΔV_{exc} and ΔV_{rec} according to Eq. (17). The baseline value of this current (that is, when $\Delta V_{exc} = \Delta V_{rec} = 0$) is 0.016 pA/pF.

Figure 6 displays some examples of the transmembrane potential time course of cell 10 (atrial cell) and 101 (nonexcitable cell). The different dynamical regimes are illustrated. It appears that the electrical activity of the nonexcitable cells tends to resemble that of the excitable cells present in their neighborhood, but with a smaller amplitude and slope, in agreement with *in vitro* recordings [6].

In order to evaluate the importance of the boundary and the finite-size effects, simulations were performed on fiber models with different lengths. Figure 7 shows bifurcation diagrams obtained with 100 excitable cells and 5, 10, and 20 nonexcitable cells respectively. A larger network of connected nonexcitable cells appears to facilitate the occurrence of spontaneous activations. This situation can be interpreted as a set of excitable cells connected to a more powerful battery.

Figure 8 presents bifurcation diagrams obtained with $M = 5$ nonexcitable cells and a number of excitable cells N ranging from 4 to 200. Increasing the number of excitable cells from 100 to 200 did not produce significantly different results, as is suggested by cell 1 being very close to its resting potential in the steady-state membrane potential profiles in Fig. 4. By decreasing the number of excitable cells N, finite-size effects were studied, which enabled a comparison with the results of the two-cell model of Sec. II. First, when N was decreased ($N < 50$ in Fig. 8), the pacemaker activity disappeared at high values of the equilibrium potential u_0 because the restoring force [Eq. (5)] was strong enough to prevent the transmembrane potential from falling down significantly below u_0 after an action potential is triggered. Second, pacemaker activity was observed for lower values of u_0 since less electrotonic current is needed to make the electrical impulse propagate in a very short fiber (see Fig. 4). Third, when M and N were both small ($N = 4$ in Fig. 8), the system did not show any pacemaker activity when g_c became high. The transmembrane potential of the excitable cells tended to a resting value near u_0. This situation is close to the dynamics of the simplified two-cell model. Note that in no case was
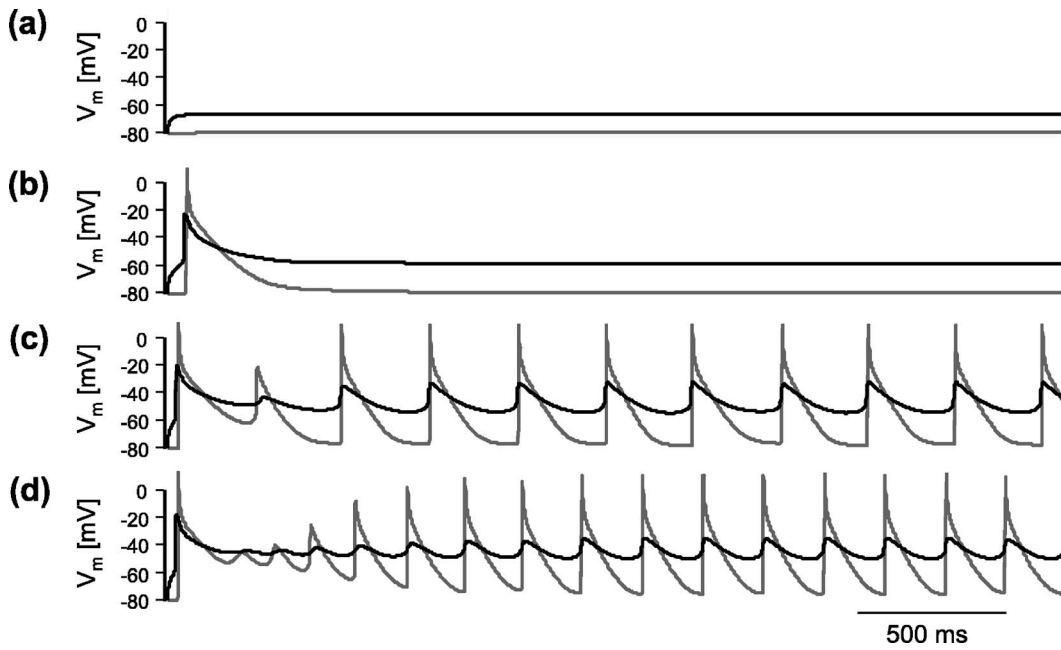
FIG. 6. Time course of the transmembrane potential of cell 10 (gray line) and cell 101 (black line) over a time interval of 3 s. The parameters are as follows: (a) $\Delta V_{exc}=-7$ mV, $\Delta V_{rec}=1$ mV, $u_0=-55$ mV; (b) $\Delta V_{exc}=-7$ mV, $\Delta V_{rec}=1$ mV, $u_0=-45$ mV; (c) $\Delta V_{exc}=-8$ mV, $\Delta V_{rec}=1$ mV, $u_0=-40$ mV; (d) $\Delta V_{exc}=-8$ mV, $\Delta V_{rec}=3$ mV, $u_0=-40$ mV; and $g_c=9$ nS/pF in all cases.

there pacemaker activity for $g_c=0$ nS/pF. Moreover, in the vicinity of the transition in the bifurcation diagram, damped oscillations similar to those of the two-cell model were observed. However, in longer fibers, the electrical impulse propagated far from the nonexcitable cells in a all-or-none fashion.

V. DISCUSSION

Several mechanisms have been proposed to explain the occurrence of ectopic foci, such as microreentries [22,23], groups of cells with auto-oscillatory dynamics [24–26], electro-mechanical coupling [27], and activations induced by electrotonicity [10]. Here, in order to evaluate the last hypothesis mentioned, we investigated the electrophysiological conditions in a biophysical model for which electrotonic effects induced by the coupling with fibrous tissue can lead to spontaneous repetitive activations.

FIG. 7. Bifurcation diagrams of the spontaneous activity of the multicellular fiber model. The same presentation and gray level code as Fig. 3 is used. The number M of nonexcitable cells included in the fiber model is (a) $M=5$, (b) $M=10$, and (c) $M=20$. In all the three cases, $\Delta V_{rec}=1$ mV and $\Delta V_{exc}=-7.5$ mV.

The results obtained in a multicellular fiber model suggest that coupling with fibroblasts facilitates the formation of focal sources triggering or perpetuating AF. However, an alteration of the excitation properties of the cells was found to be necessary for pacemaker activity to occur while keeping the values of the parameters within physiological range. This is due to the fact that the original Courtemanche model does not have a sufficiently high window current to enable repetitive firing. Whether there exists a significant sodium window current in normal or pathological cardiac cells remains an open question, because of the difficulty to directly measure this current in real cells. However, indirect evidences suggest its presence, as discussed in Keener [11].

Fibrosis seems to contribute to the creation of an arrhythmogenic substrate, but other complementary mechanisms have to be involved. This is consistent with the clinical observation that although a large proportion of the elderly have fibrosis, only a fraction of them suffer from AF. Also, in the normal heart, the density of connective tissue (fibroblasts) is higher in the sinoatrial node, the natural pacemaker, than in the rest of the atria [6,28].

This study was limited to the one-dimensional monodomain case in order to enable a sufficiently wide scanning of the parameter space. In a more realistic three-dimensional structure representing the pulmonary vein region, wave front curvature, the extracellular domain, the possible active properties of the nonexcitable cells, the complex geometry and fiber structure, possible loss of coupling or heterogeneity in tissue conductivity, and the three-dimensional distribution of fibrous tissue may induce other electrotonic effects which have to be taken into account. However, we predict that the qualitative behavior of the phenomena described in this paper will also be found in such a detailed model [10].
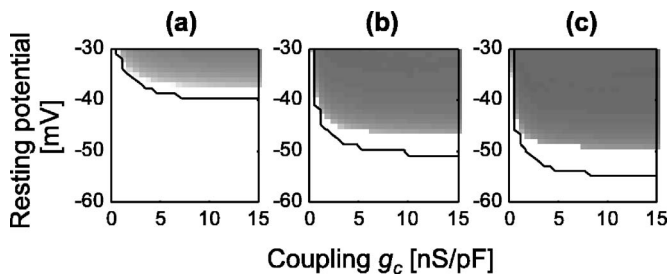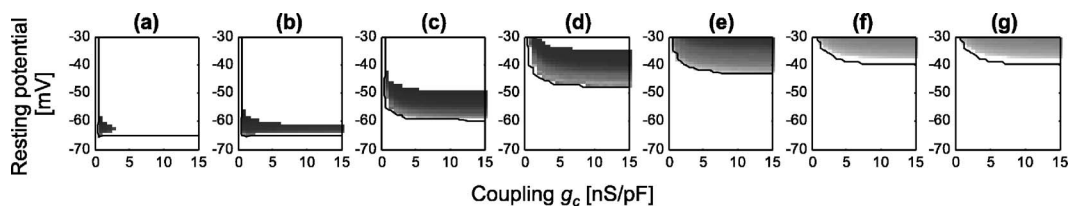
FIG. 8. Bifurcation diagrams of the spontaneous activity of the multicellular fiber model. The same presentation and gray level code as Fig. 3 is used. The number N of excitable cells included in the fiber model is (a) $N=4$, (b) $N=5$, (c) $N=20$, (d) $N=40$, (e) $N=50$, (f) $N=100$, and (g) $N=200$, and the number M of nonexcitable cells is 5. In all the three cases, $\Delta V_{rec}=1$ mV and $\Delta V_{exc}=-7.5$ mV.

VI. CONCLUSION

Pacemaker activity can arise from electrotonic effects when excitable, but nonpacemaker cells are coupled to non-excitable cells characterized by a higher resting potential. An alteration of the activation and recovery properties of the sodium channel was needed to increase the steady-state sodium current, so that these spontaneous activations can occur. This phenomenon is strengthened by a larger coupling between the excitable and nonexcitable cells, or by a higher difference in resting potential. This model may serve as a building block to develop a biophysical model of focal AF.

[1] M. Haissaguerre, P. Jais, D. C. Shah, A. Takahashi, M. Hocini, G. Quiniou, S. Garrigue, A. Le Mouroux, P. Le Metayer, and J. Clementy, N. Engl. J. Med. **339**, 659 (1998).

[2] A. S. Go, E. M. Hylek, K. A. Phillips, Y. Chang, L. E. Henault, J. V. Selby, and D. E. Singer, J. Am. Med. Assoc. **285**, 2370 (2001).

[3] M. J. Davies and A. Pomerance, Br. Heart J. **34**, 150 (1972).

[4] B. A. Sims, Br. Heart J. **34**, 336 (1972).

[5] W. C. Roberts and J. K. Perloff, Ann. Intern Med. **77**, 939 (1972).

[6] P. Camelliti, T. K. Borg, and P. Kohl, Cardiovasc. Res. **65**, 40 (2005).

[7] I. Kiseleva, A. Kamkin, A. Pylaev, D. Kondratjev, K. P. Leiterer, H. Theres, K. D. Wagner, P. B. Persson, and J. Gunther, J. Mol. Cell. Cardiol. **30**, 1083 (1998).

[8] P. Kohl, P. Camelliti, F. L. Burton, and G. L. Smith, J. Electrocardiol. **38**, 45 (2005).

[9] T. Saito, K. Waki, and A. E. Becker, J. Cardiovasc. Electrophysiol. **11**, 888 (2000).

[10] F. H. Fenton, E. M. Cherry, J. R. Ehrlich, S. Nattel, and J. Evans, Heart Rhythm **1**, S187 (2004).

[11] J. P. Keener, J. Cardiovasc. Electrophysiol. **14**, 1225 (2003).

[12] R. Plonsey and R. C. Barr, *Bioelectricity: A Quantitative Approach* 2nd ed. (Kluwer Academic, New York, 2000).

[13] R. A. FitzHugh, Biophys. J. **1**, 445 (1961).

[14] J. Nagumo, S. Animoto, and S. Yoshizawa, Proc. IRE **50**, 2061 (1962).

[15] J. M. Rogers and A. D. McCulloch, IEEE Trans. Biomed. Eng. **41**, 743 (1994).

[16] C. Rocşoreanu, A. Georgescu, and Giurgiţeanu, *The FitzHugh-Nagumo Model: Bifurcation and Dynamics*, Mathematical Modelling: Theory and Applications Vol. 10 (Kluwer Academic, New York, 2000).

[17] G. Gaudesius, M. Miragoli, S. P. Thomas, and S. Rohr, Circ. Res. **93**, 421 (2003).

[18] M. Courtemanche, R. J. Ramirez, and S. Nattel, Am. J. Physiol. **275**, H301 (1998).

[19] J. R. Ehrlich, T.-J. Cha, L. Zhang, D. Chartier, P. Melnyk, S. H. Hohnloser, and S. Nattel, J. Physiol. (London) **551**, 801 (2003).

[20] K. Kumagai, M. Ogawa, H. Noguchi, T. Yasuda, H. Nakashima, and K. Saku, J. Am. Coll. Cardiol. **43**, 2281 (2004).

[21] Y. Shibukawa, E. L. Chilton, K. A. Maccannell, R. B. Clark, and W. R. Giles, Biophys. J. **88**, 3924 (2005).

[22] E. M. Cherry, J. R. Ehrlich, S. Nattel, J. Evans, and F. H. Fenton, Heart Rhythm **1**, S85 (2004).

[23] T. R. Chay and Y. S. Lee, J. Theor. Biol. **155**, 137 (1992).

[24] D. Cai, Y. C. Lai, and R. L. Winslow, Phys. Rev. Lett. **71**, 2501 (1993).

[25] P. Parmananda, H. Mahara, T. Amemiya, and T. Yamaguchi, Phys. Rev. Lett. **87**, 238302 (2001).

[26] Y. Nagai, H. Gonzalez, A. Shrier, and L. Glass, Phys. Rev. Lett. **84**, 4248 (2000).

[27] A. V. Panfilov, R. H. Keldermann, and M. P. Nash, Phys. Rev. Lett. **95**, 258104 (2005).

[28] I. Shiraishi, T. Takamatsu, T. Minamikawa, Z. Onouchi, and S. Fujita, Circulation **85**, 2176 (1992).